# SMART MONITORING OF THE FRP COMPOSITE BRIDGE WITH DISTRIBUTED FIBRE OPTIC SENSORS

T. Siwowski[1], M. Rajchel[1], R. Sienko[2] and L. Bednarski[3]
[1] *Rzeszow University of Technology, Poland, Email:siwowski@prz.edu.pl*
[2] *Cracow University of Technology, Poland, Email: rsienko@pk.edu.pl*
[3] *AGH University of Science and Technology, Poland, Email: lukaszb@agh.edu.pl*

## ABSTRACT

Considering the worldwide recognized advantages of fibre optic sensors as measuring devices in the SHM of the FRP bridges and the unique ability to measure the long range distributed strain and temperature along the entire bridge superstructure, the distributed fibre optic sensors (DFOS) technology was chosen for the SHM system of the first Polish all-composite FRP bridge. The initial results of the SHM with the DFOS technology are the main subject of the paper. Analysis of the results obtained in the field proved the effectiveness of the distributed fibre optic sensors based on Rayleigh scattering for the SHM purposes. Wide range of practical problems related to sensor installation, fibre connection, and data processing were successfully solved in the pilot field application described in this paper. The smart DFOS sensors can ensure an acceptable measurement accuracy, thereby providing reliable strains referring to time-dependent behaviour of the FRP bridge span to assess the safety and serviceability of the all-composite bridge.

## KEYWORDS

Distributed fibre optic sensors, Rayleigh scattering, all-composite FRP bridge, monitoring.

## INTRODUCTION

The FRP composites have been used in bridge engineering for almost 35 years. Since the beginning of the 21st century, a great number of the FRP manufacturers on both sides of the Atlantic Ocean have developed and successfully implemented many FRP composite systems for bridge construction and maintenance. Many of these bridges are still being monitored to evaluate service performance of this emerging technology and, simultaneously, many of the next FRP construction products are being tested in various research projects worldwide. Fibre optic sensors (FOSs) in general have been often proposed to substitute the traditional electronic sensors in SHM applications. Initially, fibre optic sensing technology has advanced and matured as a spin-off of optical telecommunication developments. Many types of sensors have been developed with various characteristics. Common approaches use interferometry, Bragg gratings, scattering mechanisms, and fluorescence (Udd 1995). They all benefit from the low profile and low loss of optical fibre. The sensors can be placed in difficult locations and the information can be sent over long fibre tubes. This results in a permanent, flexible capability of non-destructive testing. Moreover, by incorporating sensing devices, the development of such structurally integrated FOSs and intelligent sensing has led to the concept of smart structures.

Over the past several years, there have been many new opportunities for applying various FOS technologies in the FRP bridge field demonstration projects. For example, the fibre optic Bragg grating (FBG) sensors were installed during the fabrication of one of the first FRP bridge worldwide – the West Mill Bridge in England – as a part of the structural monitoring system (Kister et al. 2007). Watkins gives an overview of two FOS equipped FRP bridges. The sensing system in one application monitors general performance and health of the structure, while the system in the second application tracks the behaviour of a major structural repair. A few from many the FRP bridge projects being currently health-monitored in Canada, are described in Tennyson et al. (2000). In these projects, the FBG strain and temperature sensors were mostly used to monitor structural behaviour during construction and under serviceability conditions. Since many applications of FOS technology have been successfully implemented and tested, the FOS sensor has become broadly accepted as a structural health monitoring device for the FRP materials by either embedding into or bonding onto the structures.

Recent advances in FOS technologies have fostered the development of innovative solutions for the health monitoring of civil engineering structures. The linear Rayleigh scattering and nonlinear Brillouin or Raman scattering are currently being used together with optical reflectometric and signal processing techniques to track the fibre transducer. Distributed fibre optic sensors (DFOS) based on Rayleigh, Brillouin or Raman scattering add an unique ability to measure the long range distributed strain and temperature along standard telecom-grade optical fibres, otherwise attainable in a quasi-distributed fashion only with several sensors applied at discrete locations.

In addition, an access to only one end of the circuit is required, thereby enabling measurements even in case of damage or interruption of the sensing circuit at a random point. The technology holds significant potential for the health monitoring of large structures, including bridges (Matta et al. 2008; Galindez – Jamioy and Lopez – Higuera 2012). The distributed FOS technology is capable to measure simultaneously the strain level and locate the strained point along the sensor. This feature, which has no performance equivalent among the traditional electronic sensors, is considered to be extremely valuable. When the sensors are properly installed on the most significant structural elements, the system can lead to the comprehension of the real static behaviour of the structure rather than merely measure the discrete strain level on one of the structural elements. In addition, the sensor required by DFOS technology is an inexpensive, telecom-grade optical fibre that shares most of the typical advantages of FOS, such as high resistance to moisture, corrosion and electro-magnetic fields.

Considering the worldwide recognized advantages of FOSs as measuring devices in the SHM of the FRP bridges and the unique ability to measure the long range distributed strain and temperature along the entire bridge superstructure, the DFOS technology was chosen as the basic technology for the SHM system of the first Polish FRP composite bridge. However, the validation of the DFOS techniques is critical to address the development of monitoring systems with improved accuracy and spatial resolution tailored for the FRP bridge applications. To ensure the accurate and reliable DFOS readings, two additional monitoring techniques were also implemented in case of this bridge, i.e. acoustic emission and vibrating string gauges (Karczewski et al. 2015). All three monitoring techniques are still trailing on site continuously. The initial results of the SHM with the DFOS technology for the first Polish FRP bridge are the main subject of the paper.

## FRP BRIDGE DESCRIPTION

The first Polish road bridge fully made of FRP composites is situated in Rzeszow, the capital of Podkarpackie voivodeship, along the urban road over a small local stream. This is a 10.7 m long single-span simply supported bridge with 7.7 m wide deck, carrying 2 × 2.5 m wide roadway and two 0.75 m and 1.1 m wide sidewalks. Its nominal carrying capacity amounts 30 metric tonnes according to the Polish bridge standard. The all-composite bridge superstructure is formed by four FRP composite girders with an overlying 0.13 m thick FRP sandwich deck slab (Fig. 1). The deck equipment consists of two lightweight concrete sidewalk slabs reinforced with GFRP bars and encompassed by stone curbs and polymer cornice plates, thin insulation and pavement layer, two expansion joints and steel balustrades. Eight elastomer bearings are used to support the FRP span on the RC abutments. The solid abutments are placed on 10 micropiles with diameter of 110 mm and length of 4.0 m (Fig. 2).

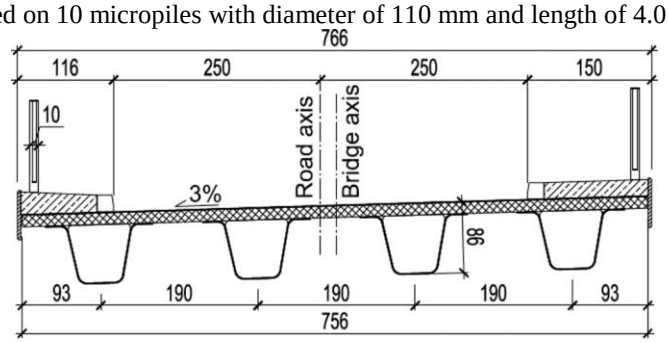


*Figure 1: Cross-section of the bridge superstructure (units: cm)*

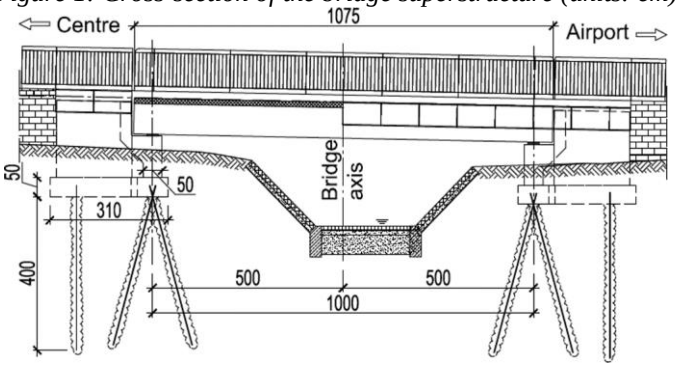


*Figure 2: Side view and longitudinal section of the bridge (units: cm)*

The FRP girders have a box cross-section with slightly inclined webs, two top 220 mm wide and 15 mm thick flanges and one bottom 340 mm wide and 15 mm thick flange. The maximum width of the girder amounts 1380

mm and the depth is 715 mm. The top and bottom flanges are made of solid GFRP composites whereas the webs are made in form of the sandwich panels with PVC foam layer between two GFRP laminates. To increase the torsional stiffness of the FRP girder and to prevent buckling of webs, nine internal diaphragms are placed and bonded along the length of the girder. The diaphragms are made in form of 46 mm thick sandwich plates with a structure similar to the webs. The sandwich bridge deck slab consists of two 11,5 mm thick external laminates and 105 mm thick PUR foam core stiffened with the internal vertical ribs. The deck panels are made of the GFRP composite and are bonded to the top flanges of each girder with epoxy adhesive.

The unidirectional and biaxial stitched glass fabrics were used as a reinforcement of the FRP composites in the superstructure. The weight of glass fabrics ranged from 800 to 1200 g/m$^2$. As a core material for sandwich parts of girders and deck panels, the PVC foam with density of 80 kg/m$^3$ and the PUR foam with density of 105 kg/m$^3$ were applied respectively. The matrix of all composite parts was made of epoxy resin.

## MONITORING SYSTEM

For distributed strain and temperature measurements, the optical reflectometer based on linear Rayleigh scattering called Luna OBR 4600 was used (Samiec 2012). This reflectometer enables ultra high resolution reflectometry with backscatter level sensitivity. The OBR 4600 has spatial resolution as fine as 10 microns and no dead zone. It comes with an extensive range of options including a strain and temperature sensing package with maximum sensor length up to 2 kilometres. Distributed strain and temperature measurements are made by sensing the spectral shift in the fibre Rayleigh scatter. The OBR uses swept-wavelength interferometry (SWI) to measure the Rayleigh backscatter as a function of length in optical fibre with high spatial resolution. Rayleigh backscatter in optical fibre is caused by random fluctuations in the index profile along the fibre length. Scatter amplitude is a random but static property of a given fibre and can be modelled as a continuous weak fibre Bragg grating (FBG) with a random period. Changes in the local period of the Rayleigh scatter cause temporal and spectral shifts in the locally-reflected spectrum. These shifts can then be scaled to form a distributed sensor. This SWI-based technique enables robust and practical distributed temperature and strain measurements, with millimetre-range spatial resolution over tens to hundreds of meters of standard fibre, with strain and temperature resolution amounting 1 με and 0.1 °C respectively.

The single-mode telecom-grade optical fibres were applied and 10 mm virtual measurement sections spaced every 10 mm along optical fibres were set to measure the strain and temperature. The fibres installation took place in the workshop just after the composite girders and deck panels were manufactured. The optical fibres were placed inside two bridge girders and bonded to their composite body as seen in Fig. 3. Ten sensors were installed on the girder and one optical fibre with the loop was mounted on the girder's end of thus creating two sensors. The length of one optical fibre sensor was about 9.60 ± 0.10 m and strain measurements were carried out in almost 20 000 virtual discrete points of the girder (table 1). The section of the sensor no. 10 was placed inside a polypropylene tube in order to measure the ambient temperature during testing to compensate its influence on strain readings.
One deck panel with dimensions of 5.35 x 1.92 m was equipped with the optical fibre sensors. Two fibres were installed on the top and bottom composite surfaces of the panel, i.e. sensors no. 01/02 and 03/04, respectively. Their alignment enabled to measure strains in both transverse and longitudinal directions of the panel (Fig.3). The exact location of the monitored girders as well as the deck panel in the FRP bridge superstructure is shown in Fig.4.

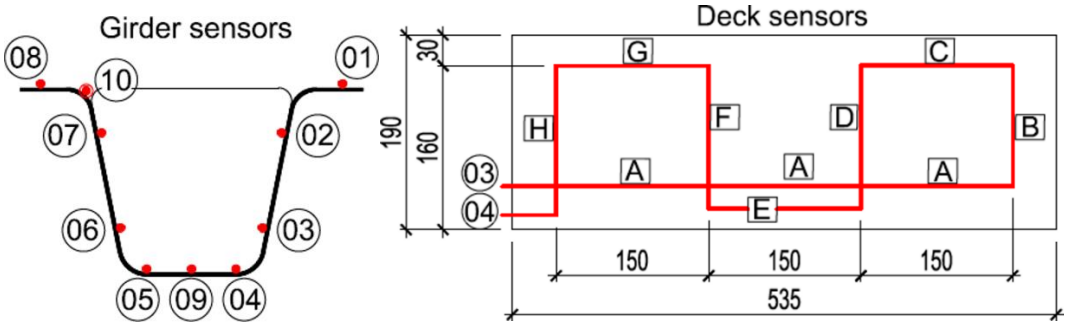


*Figure 3: Sensor layout for the girder and deck panel strains measurement (sensor no. 10 for temperature only)*

Table 1: Number of virtual discrete points of strain measurements

| Superstructure element | Sensor | No. of measurement points |
|---|---|---|
| Girder no. G1 (main sensors) | 04 | 927 |
| | 05 | 947 |
| | 08 | 968 |
| | 09 | 966 |
| Deck panel | 03/A | 439 |
| | 03/B | 104 |
| | 03/C | 120 |
| | 03/D | 149 |
| | 03/E | 100 |
| | 03/F | 142 |
| | 03/G | 90 |
| | 03/H | 105 |

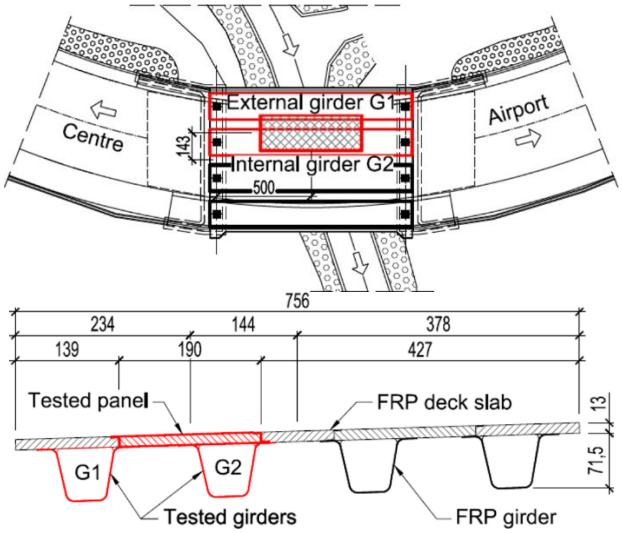


*Figure 4: Location of the monitored girders and the deck panel in the FRP bridge superstructure*

## PROOF LOAD TESTS

The bridge monitoring was planned as a sequence of several proof load tests under controlled loading carried out twice a year during first five years of the bridge service period. The first proof test was carried out just after completion of the bridge and before it was opened to traffic, in November 2016. The results of this testing were also the basis to obtain the relevant service permit from the local road authority. Therefore except DFOS, the conventional discrete foil strain gauges, accelerometers, as well as LVDTs were also used in most of critical locations of the FRP superstructure. Thus two different strain measurement techniques applied for testing enabled the validation of the DFOS measurement by comparing the strains resulting from both techniques. The second proof load test was carried out under the same loading conditions in June 2017 and the traffic was stopped for a few hours to facilitate testing.

In both proof load tests two, four-axle heavy vehicles were used as a bridge loading with the total mass of 64220 kg in the first test and 64340 kg in the latter one (the difference less than 0.2% is negligible for comparison purposes). The location of two vehicles on the bridge superstructure is shown in Fig.5. Before vehicles entered the bridge, the strain readings were adjusted for 0 value as a reference line for comparison purposes. The following strain readings were carried out in two loading stages: under the full loading of the bridge (maximum strains) and few minutes after unloading (residual strains). The temperature induced strains were compensated due to temperature strain measurement with the optical fibre sensor no. 10. The ambient temperature differences in various stages of both tests amounted about 1 - 3 °C, which meant the strains in the range of 30 - 100 με (microstrains) ought to be deducted in final strain evaluation.

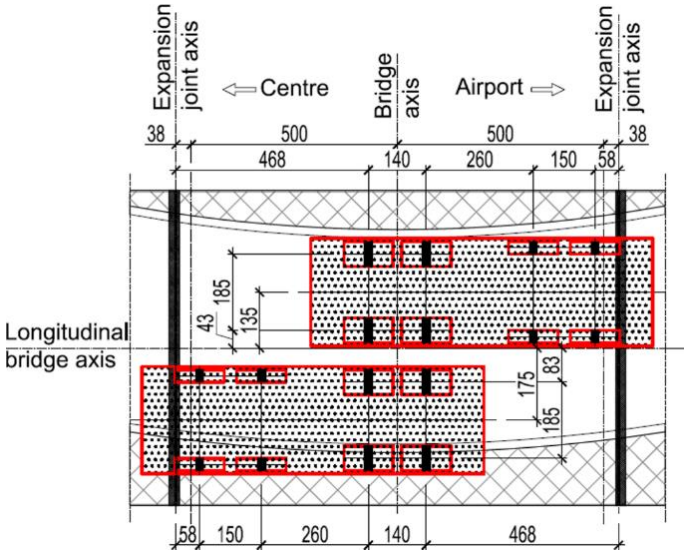


*Figure 5: Location of proof load on the bridge*

## MONITORING RESULTS

In the following graphs, the strain measurements along selected fibre optic sensors are presented. The positive (+) values mean the tensile strains, while the negative ones – the compression strains detected in the relevant discrete locations along the fibres. The graphs comprise strains measured in both loading tests for better comparative analysis. This comparison allows to evaluate the FRP superstructure performance during first several months of service to check both traffic and environment influence on the structural behaviour of the bridge. The comparison reveals qualitatively and quantitatively the strain differences induced during service and, on their basis, the current state of repair of the bridge can be monitored. Except the static strain measurements made with the DOFS, the supplementary vibration measurement with accelerometers was also carried out for monitoring purposes to evaluate the modal characteristic of the bridge after several months of service. The results of the modal analysis are not reported in this paper.

Figs 6 and 7 present strains detected in the bottom flange of the external girder measured with fibre optic sensors no. 05 and no. 09. In turn, Fig.8 shows the graph of the strains in the upper flange of the same girder measured with fibre optic sensor no. 08. Both, positive and negative strain values were detected in this location. In Fig. 9 the graph of the strains measured on the bottom surface of the deck panel (sensor no. 03/04) is presented. Several strain sections, depending on the sensor division, are shown with the reference to Fig.3. Both tension/compression and transverse/longitudinal strains induced in the deck panel under loading are presented.

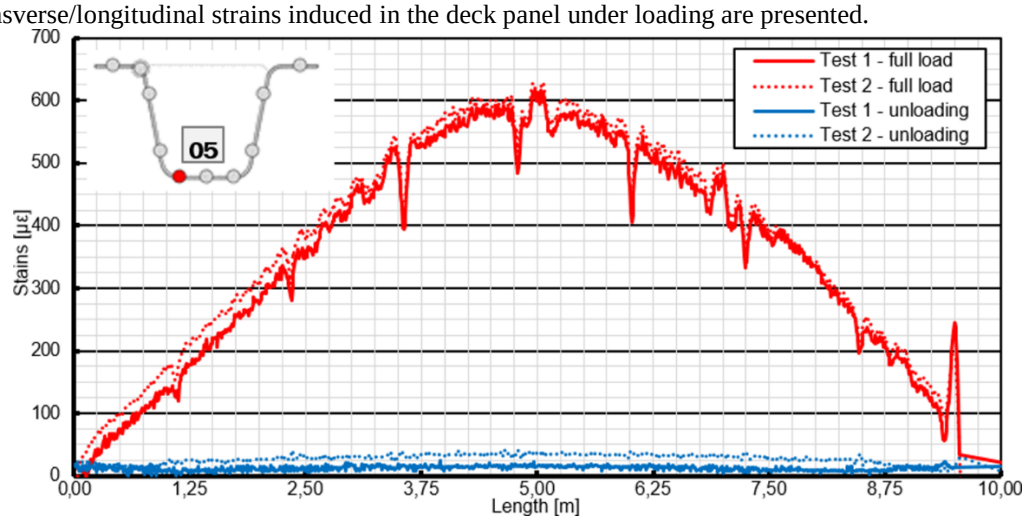


*Figure 6: Graph of the strains measured with the DFOS no. 05 – the bottom flange of G1*

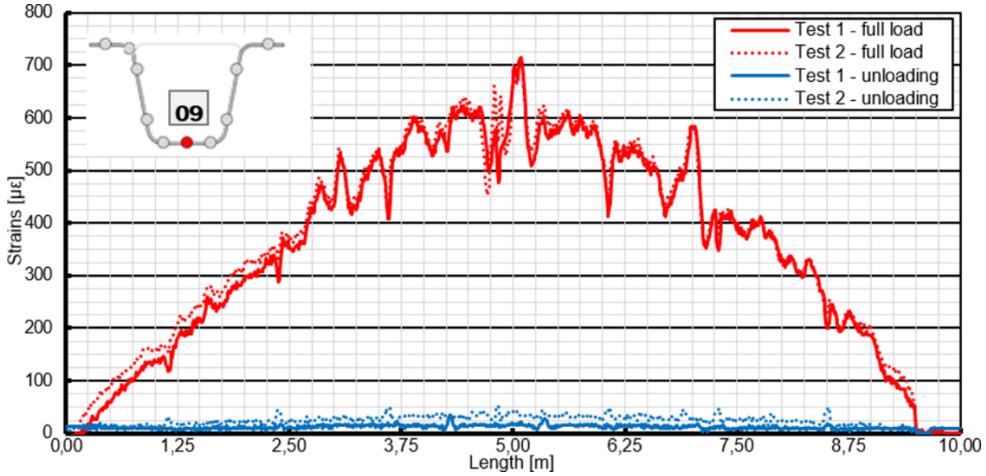


*Figure 7: Graph of the strains measured with the DFOS no. 09 - the bottom flange of G1*

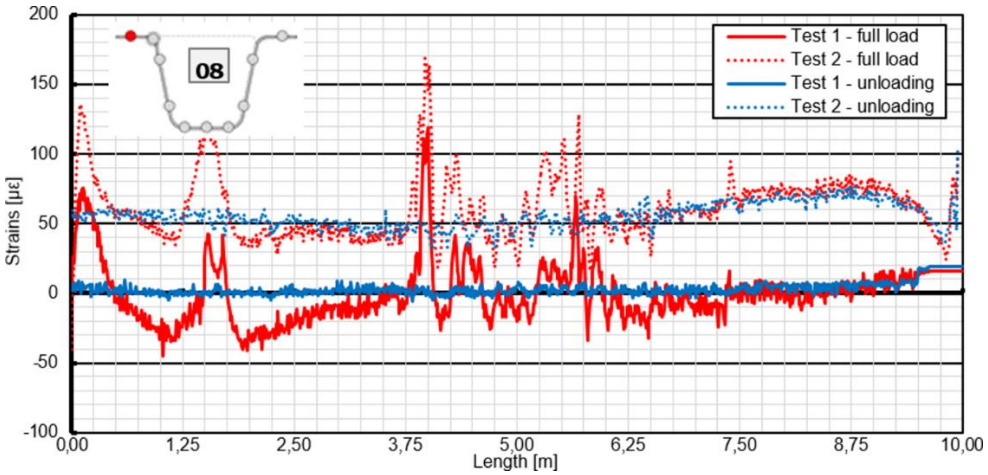


*Figure 8: Graph of the strains measured with the DFOS no. 08 – the upper flange of G2*

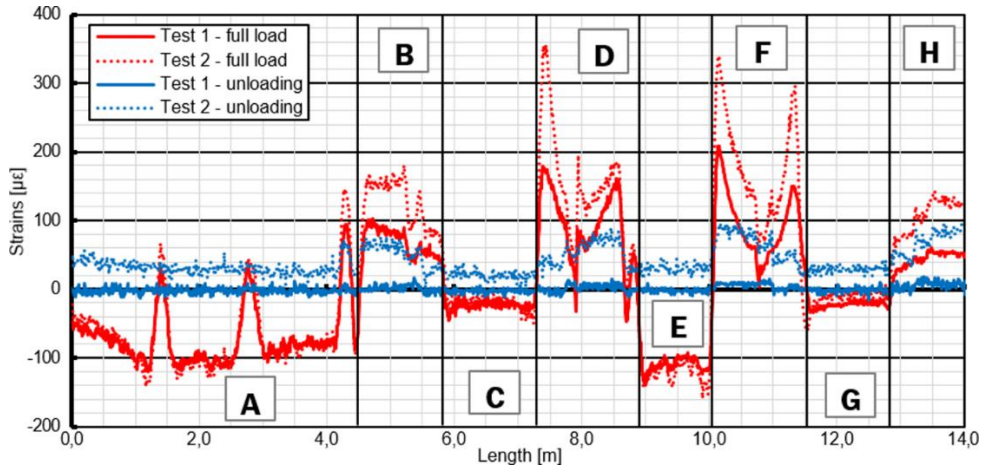


*Figure 9: Graph of the strains measured with the DFOS no. 03 - the bottom surface of the deck panel*

## DISCUSSION

Comparing the strain graphs of both girders obtained in the test 1 and test 2, it can be concluded that their character and strain values are very similar, which reveals no negative influence of traffic load and environment on the girders behaviour after 8 months of bridge service. It should be emphasized that the strain of 100 x $10^{-6}$ (denoted 100 με) corresponds to the stresses ranging 1,21-4,21 MPa, depending on the lamina type in each composite. The

only considerable difference was detected in sensor no. 08 mounted on the upper flange of the girder's U-body. The characteristic sharp changes of the strain plots indicate the girder's sections where the diaphragms are located. The diaphragms, glued inside the girder U-body, sharply decrease strains in adjacent composite laminates.

The maximum strain in bottom flange of the G1 girder was about 715 με in both tests (sensor 09). After the bridge unloading, the remaining strains amounted only 30 and 50 με in test 1 and 2 respectively. The maximum strains measured by the sensors no. 05 and no. 09 revealed that they are not constant across the flange width. The axis strain (sensor no. 09) was about 100 με greater than the edge strain (sensor no. 05), which indicates the small shear lag effect in the bottom flange. The mean differences between strains in tests 2 and 1 ranged only 12-18 με (sensors no. 09 and no. 05), which showed the lack of any negative effect during 8 months of service.

The strains in the upper flange of the G1 girder (sensor no. 08) oscillated around 0 and were both positive and negative in the test 1. The maxima on both sides amounted about 120 με and -45 με respectively. It indicates that the location of girder's neutral axis seems to be in the bond line between girder's U-body and the deck panel. In the test 2, the strains measured in sensor 08 increased by 50-60 με in average and were only positive (tension). The maximum strain was about 170 με. It was due to additional strains induced by the temperature. During the second bridge test, the ambient temperature was about 25 °C and as a result, the temperature of the FRP panel was much higher due to black thin pavement layer. The mean reading of thermal sensor 10 was about 60 με during the entire test. This strain increase due to temperature was visible only in higher part of the girder (deck, upper flanges) and disappeared towards bottom flange, where no thermal effect was detected.

The behaviour of the deck panel was identified on the basis of the sensor no. 03 strain measurement. It was located on the external bottom surface of the panel and enabled the strain detection in both panel directions. The strains along the A section parallel to the panel longitudinal axis indicate that the location of the girder's neutral axis is a little below the bond line (full compression of the deck in longitudinal direction). The maximum compression strain was about -100 με and increased to 0 after bridge unloading. The mean difference between maximum strains in both tests amounted only 5 με is negligible, which confirms the identical panel behaviour under load in both tests. The bigger strain difference was detected after unloading (about 30 με), because the bigger remaining strains were left in the panel after test 2. The strains along the C and G sections, also parallel to the panel longitudinal axis, were smaller than corresponding A section strains. In this part of the panel, the sensor no. 03 was located inside the U-girder and the maximum strains on the panel bottom surface ranged -30 till -45 με. The mean difference between maximum strains in both tests was only 3-13 με and about 30 με after unloading.

The transverse strains induced by panel bending between G1 and G2 girders were measured along the sections B, D, F and H by the sensor no. 03. These strains were twice as large as in case of the longitudinal sections and had positive values which indicates tension of the panel's bottom surface. The maximum strains were measured along the D and F sections (close to the middle of the panel), and their maximum values ranged 180-200 με and 340-360 με in the test 1 and 2 respectively. The mean strain increase along these sections amounted about 60-80 με under full loading and 50-60 με after unloading. It confirms the thesis about additional thermal strains in the deck panel. A little lower strain increase was detected along sections B and H, where the mean strain increase between two tests ranged 45-65 με, both under and after loading. However, the maximum strains in the test 2 were twice smaller than in the test 1 and equalled 140-180 με.

To summarize, the DFOS strain measurements of the FRP bridge span during two load tests in the space of 8 months reveal the very safe stress level in the FRP elements and strain differences having no practical meaning, referring to time dependent behaviour of the bridge span. The maximum strain detected during both tests was about 845 με, which corresponds to the stresses in particular laminas ranging 10.2 – 35.6 MPa and which, in turn, is about 4.2 – 8.0 % of their tensile strength. After 8 months of service, excluding momentary thermal strains, no serious changes in the FRP composite superstructure behaviour were observed under full loading and after unloading. The maximum difference between strains, measured during test 1 and 2, was about 80 με and is negligible referring to safety and serviceability of the all-composite bridge. However, it confirms the necessity of monitoring such kind of prototypes, where not fully proven structural and material solutions were applied.

## CONCLUSIONS

The FRP composites, considered as a new generation of structural materials for bridges, offer great opportunities by contributing to construction of high-performance third-generation structures, which may be expected to be durable, i.e. highly resistant to environmental degradation over time, and smart, i.e. able to continuously monitor their own state of health. Moreover, in order for changes in bridge design and construction to be accepted, it is necessary to health-monitor the innovative structures. To assist in achieving this goal, the RUT has developed a

new approach, which integrates civil engineering and electrophotonics. As a result of the project, the participating engineers have now the knowledge to build "smart" FRP structures equipped with the SHM technology to provide much needed information related to the health of structures before any failure occurs.

Analysis of the results obtained in the field proved the effectiveness of the distributed fibre optic sensors based on Rayleigh scattering for the SHM purposes. Wide range of practical problems related to sensor installation, fibre connection, and data processing were successfully solved in the pilot field applications described in this paper. The smart distributed fibre optic sensors can ensure an acceptable measurement accuracy, thereby providing reliable strains referring to time-dependent behaviour of the FRP bridge span to assess the safety and serviceability of the all-composite bridge.

## ACKNOWLEDGMENTS

This research project was supported by the Polish National Centre of Research and Development (NCBiR), within the framework of DEMONSTATOR+ program; the project title: "Com-bridge: Innovative road bridge with FRP composites" (No. UOD-DEM-1-041-/001).

## REFERENCES

C.A. Galindez – Jamioy, J.M. Lopez - Higuera (2012). "Brillouin distributed fiber sensors: an overview and applications", Hindawi Publishing Corporation Journal of Sensors, article ID 204121, 17 pages.

R. Karczewski, Ł. Gołębiowski, R. Molak, J. Płowiec, W.L. Spychalski (2015). "Acoustic emission in monitoring composite bridge structures", Composites Theory and Practice, 15, 112-116.

G. Kister, R.A. Badcock, Y.M. Gebremichael, W.J.O. Boyle, K.T.V. Grattan, G.F. Fernando, L. Canning (2007). "Monitoring of an all-composite bridge using Bragg grating sensors", Construction and Building Materials, 21, 1599-1604.

F. Matta, F. Bastianini, N. Galati, P. Casadei, A. Nanni (2008). "Distributed strain measurement in steel bridge with fiber optic sensors - validation through diagnostic load test", Journal of Performance of Constructed Facilities, 22, 264–273.

D. Samiec (2012). "Distributed fibre-optic temperature and strain measurement with extremely high spatial resolution", Photonic International, 10-13.

R.C. Tennyson, T. Coroy, G. Duck, G. Manuelpillai, P. Mulvihill, David J.F. Cooper, P.W.E. Smith, A.A. Mufti, S.J. Jalali (2000). "Fibre optic sensors in civil engineering structures", Canadian Journal of Civil Engineering, 27, 880–889.

E. Udd (1995). "Fiber Optic Smart Structures", Wiley, New York.

S.E. Watkins (2003). "Smart bridges with fiber – optic sensors", IEEE Instrumentation & Measurement Magazine, 6, 25-30.